

Heterodyne Spectroscopy of the 63 μm O I Line in M42

R. T. Boreiko and A. L. Betz

Center for Astrophysics and Space Astronomy, University of Colorado, Boulder, CO 80309

ABSTRACT

We have used a laser heterodyne spectrometer to resolve the emission line profile of the 63 μm $^3P_1 - ^3P_2$ fine-structure transition of O I at two locations in M42. Comparison of the peak antenna temperature with that of the 158 μm C II fine-structure line shows that the gas kinetic temperature in the photodissociation region near $\theta^1\text{C}$ is 175 - 220 K, the density is greater than $2 \times 10^5 \text{ cm}^{-3}$, and the hydrogen column density is about $1.5 \times 10^{22} \text{ cm}^{-2}$. A somewhat lower temperature and column density are found in the IRc2 region, most likely reflecting the smaller UV flux. The observed width of the O I line is 6.8 km s^{-1} (FWHM) at $\theta^1\text{C}$, which is slightly broadened over the intrinsic linewidth by optical depth effects. No significant other differences between the O I and C II line profiles are seen, which shows that the narrow emission from both neutral atomic oxygen and ionized carbon comes from the PDR. The O I data do not rule out the possibility of weak broad-velocity emission from shock-excited gas at IRc2, but the C II data show no such effect, as expected from non-ionizing shock models.

Subject headings: infrared:ISM:lines, line:profiles, ISM:individual:M42

1. Introduction

Photodissociation regions (PDR) occur at the interface between H II regions and cooler molecular material. They are most easily studied via the fine-structure line emission from C^+ and O and the rotational lines of the abundant CO molecule. Of particular interest are the fine-structure lines of O I at 63 μm and C II at 158 μm , since these are believed to be the major cooling lines, with O I emission usually dominant at densities typical of dense molecular clouds ($n > 10^4 \text{ cm}^{-3}$) and C II emission more significant at lower densities (Tielens and Hollenbach 1985a). Since the ionization potential of O is very similar to that of H, essentially all the oxygen in a PDR will be neutral. Similarly, since the first ionization potential of C is similar to the dissociation energy of CO while its second ionization potential is close to that of He, carbon throughout the PDR will be singly ionized. Observations of both major fine-structure cooling lines from the same region provide information on the temperature, density, and relative abundance of the species within the PDR.

Both the $63 \mu\text{m } ^3P_1 - ^3P_2$ O I and the $158 \mu\text{m } ^2P_{3/2} - ^2P_{1/2}$ C II lines have been previously observed and mapped in Orion (e.g. Melnick, Gull, and Harwit 1979, Storey, Watson, and Townes 1979, Werner et al. 1984, Crawford et al. 1986, Stacey et al. 1993). While comparison of integrated intensities and an assumed linewidth for both transitions allowed these authors to make the first estimates of physical conditions, a definitive determination was hampered by the inability to resolve line profiles. The 5 km s^{-1} (FWHM) linewidth of the C II line near $\theta^1\text{C}$ in M42 was first measured by Boreiko, Betz, and Zmuidzinas (1988), who examined the dynamics of the photoionized gas. This Letter describes observations of the $63 \mu\text{m } ^3P_1 - ^3P_2$ line of O I in the Orion region with 0.2 km s^{-1} resolution, which gives the first fully resolved line profiles for M42 at this wavelength. Comparison with $158 \mu\text{m}$ C II line profiles at similarly high resolution allows the determination of the optical depth in both these lines, and hence the temperature and limits to the density within the PDR.

2. Instrumentation and Calibration

The data were obtained using a far infrared heterodyne receiver (Betz and Boreiko 1993) flown aboard the Kuiper Airborne Observatory (KAO). The local oscillator (LO) is the 4751.3409 GHz transition of $^{13}\text{CH}_3\text{OH}$ (Henningsen and Petersen 1978), which is 6.6 GHz away from the rest frequency of the O I line at 4744.777 GHz (Zink et al. 1991). The mixer is a GaAs Schottky diode (University of Virginia type 1T15) operated at room temperature in a corner-reflector mount. The system noise temperature measured during the observations was $140,000 \text{ K}$ (SSB). The IF signal is analyzed by a 400-channel acousto-optic spectrometer (AOS) with a channel resolution of 3.2 MHz (0.2 km s^{-1}) and bandwidth of 80 km s^{-1} at the O I frequency. The $158 \mu\text{m}$ C II spectra used for comparison with the O I data were taken in 1991 November with a system noise temperature of 9500 K (SSB) and a chopper throw of $12!5$. Other technical details are similar to those presented by Boreiko et al. (1988), with the addition of the AOS for signal analysis.

The O I observations were done using sky shopping at 4 Hz , with an amplitude of $7!5 - 8'$, which is sufficient to ensure negligible emission in the reference beam (see the map of Werner et al. 1984). The telescope beam size was $17''$ (FWHM) and the pointing accuracy is estimated to be $\sim 15''$. Absolute intensity calibration is derived from spectra of the Moon, for which a physical temperature of 394 K and emissivity of 0.98 are adopted (Linsky 1973). Conversion from DSB to SSB intensity was performed using the calculated transmission of the pressure window and the atmosphere in the two sidebands, corrected for the different source and lunar elevation angles. The net calibration uncertainty for a source filling the beam is $\leq 15\%$. The velocity scale accuracy, determined from the known line and LO rest frequencies, is better than $\pm 0.15 \text{ km s}^{-1}$ (1σ).

3. Observations

The O I line was observed from the KAO flying at an altitude of 12.5 km on the nights of 1995 Sept 9 and Sept 11. Data were obtained at two locations within the M42 complex: $\theta^1\text{C}$ and IRc2 . The Earth’s orbital velocity and the intrinsic source V_{LSR} combined to produce a net observational Doppler shift near 2 km s^{-1} , so that atomic oxygen in the Earth’s thermosphere produced an optically thick absorption line within the Orion spectra. The terrestrial line, however, is very narrow, with a velocity width of 1.3 km s^{-1} (FWHM) as determined from the lunar spectra. The Orion data were corrected for the absorption over the range of $>50\%$ transmission, while the remaining few affected channels were removed from the spectra. The interfering telluric line does not compromise the calibration accuracy or the determination of the emission line profile, since the telluric absorption profile was well measured from the lunar spectra. Also, it affects fewer than 10 of the approximately 70 resolution elements across the emission line in Orion (see Fig. 1).

Table 1 presents various parameters of the observed spectra. The continuum level is obtained from an average over all the spectral channels excluding the emission line. The peak O I antenna temperature T_r^* (as defined by Kutner and Ulich 1981) is the average value of the strongest 1.0 km s^{-1} for $\theta^1\text{C}$ and 0.6 km s^{-1} for IRc2, while that for C II is the peak measured single-channel value. The widths are measured from the raw data since the line shapes for both O I and C II are not Gaussian to within statistical uncertainty. Velocity limits for the integrated intensity are $\Delta v(\text{FWHM})$ on either side of line center.

The measured O I continuum given in Table 1 is in good agreement with that obtained from a map by Werner et al. (1976) at $\theta^1\text{C}$, but is a factor of 2.5 higher at IRc2. The most likely explanation for the apparent discrepancy is the different beamsizes of the observations, $17''$ here vs $1'$ for the data of Werner et al. (1976). A continuum source size of $\sim 40''$ FWHM, similar to that seen in $119 \mu\text{m}$ continuum data (Betz and Boreiko 1989), would reconcile the measured values. The integrated intensity values of Table 1 are in good agreement with those reported previously (Storey, Watson, and Townes 1979, Werner et al. 1984, Crawford et al. 1986).

4. Analysis and Interpretation

4.1. Gas Kinetic Temperature

Figure 1 presents spectra of the $^3P_1 - ^3P_2$ O I and the C II $^2P_{3/2} - ^2P_{1/2}$ fine-structure lines taken with the same instrument toward $\theta^1\text{C}$. A lower limit to the gas kinetic temperature of 165 K is given by the peak brightness temperature of the O I line. However, because of the high critical density of the $^3P_1 - ^3P_2$ transition ($n_c \sim 5 \times 10^5 \text{ cm}^{-3}$), the gas temperature may be higher unless the PDR has sufficient density or the line has significant optical depth. The C II transition has a much lower critical density, $n_c \sim 3 \times 10^3 \text{ cm}^{-3}$, and thus is generally in LTE. Comparison of just the two peak brightness temperatures shows that the C II line must have an optical depth $\tau < 1.6$.

Figure 2 presents curves showing the combinations of gas kinetic temperature, density, and column density of hydrogen which produce the observed peak antenna temperatures for the 63 μm O I and 158 μm C II lines at $\theta^1\text{C}$. The horizontal axis gives column density of hydrogen per unit velocity interval in a LVG model. Relative abundances of O and C are assumed to be 5×10^{-4} and 3×10^{-4} , respectively. The rate coefficients of Launay and Roueff (1977) and A coefficients of Fischer and Saha (1983) for O I were used in a statistical equilibrium escape probability formalism. Only an LTE solution is shown for the C II curve. As can be seen from the figure, consistency with both observations requires that the PDR gas temperature be less than 250 K for moderate densities, $n_{\text{H}} > 1 \times 10^5 \text{ cm}^{-3}$. An additional constraint to the allowed range of temperature and density is provided by the 145 μm $^3P_0 - ^3P_1$ O I line. Although fully resolved spectra for this higher excitation line are not available, its integrated intensity has been measured to be $(4.0 \pm 1.3) \times 10^{-3} \text{ erg cm}^{-2} \text{ s}^{-1} \text{ sr}^{-1}$ at $\theta^1\text{C}$ (as quoted by Stacey et al. 1993; a 30% uncertainty has been assumed). This relatively high value by itself excludes all potential solutions from Fig. 2 for which $n < 1 \times 10^5 \text{ cm}^{-3}$, since the critical density for this transition is $6 \times 10^4 \text{ cm}^{-3}$. Although no combination of parameters can reproduce all the observed intensities simultaneously, the best agreement is found at the higher densities, $n \geq 5 \times 10^5 \text{ cm}^{-3}$, where the 63 μm O I line has moderate optical depth. The lowest density for which a consistent solution is possible within calibration uncertainties and 1σ statistical uncertainty for all the data is $n_{\text{H}} = 2 \times 10^5 \text{ cm}^{-3}$, with $T_{\text{kin}} = 220 \text{ K}$ and $N_{\text{H}}/\Delta v = 2.8 \times 10^{21} \text{ cm}^{-2} (\text{km s}^{-1})^{-1}$. Densities of $n_{\text{H}} > 10^6 \text{ cm}^{-3}$ such that the O I lines are thermalized are also consistent with all the data to within statistical and calibration uncertainties. Thus, with no further constraints, the optical depth in the O I 63 μm line is between 2.6 and 5.3, while that for the 158 μm C II line is 1.0 - 1.3. If the abundance of oxygen relative to carbon is higher than the 5:3 ratio assumed for the calculations, then the 63 μm line optical depth would be increased and a brighter 145 μm O I line would be predicted. However, this would not change the basic conclusion that the PDR near $\theta^1\text{C}$ is characterized by $T_{\text{kin}} \leq 220 \text{ K}$, $n_{\text{H}} \geq 2 \times 10^5 \text{ cm}^{-3}$, and $N_{\text{H}} \sim 1.5 \times 10^{22} \text{ cm}^{-2}$. Additional constraints on these parameters are presented in section 4.2.

Equivalent calculations at the IRc2 position have the same difficulty reproducing the reported high 145 μm O I integrated intensity simultaneously with the low peak 63 μm O I antenna temperature. It should be noted that calibration of the 145 μm emission is difficult because it lies on the edge of a strong atmospheric feature. Again, the best solutions are found at the lower temperatures, $140 \text{ K} \leq T_{\text{kin}} \leq 180 \text{ K}$, with densities $n_{\text{H}} \geq 1 \times 10^5 \text{ cm}^{-3}$, and $n_{\text{H}}/\Delta v = (1.9 - 2.7) \times 10^{21} \text{ cm}^{-2} (\text{km s}^{-1})^{-1}$. The higher densities and column densities are associated with lower kinetic temperatures. The optical depth in the 63 μm O I line lies between 3.6 and 5.1, while that in the 158 μm C II line is 0.8 - 1.4 .

4.2. Line Width and Optical Depth

The C II line at both observed locations is narrower than the O I line by 25-40%. If the differences were due to the different beamsizes (44'' for C II vs 17'' for O I) or critical densities for

the two lines, one would generally expect the opposite effect. Therefore it is reasonable to assume that the major cause of the greater O I line width is a larger optical depth. For $\tau_{\text{C II}}$ between 1.0 and 1.3 (the range appropriate to the solutions at $\theta^1\text{C}$ discussed above), the relative linewidths of the two transitions suggest that $\tau_{\text{O I}, 63\ \mu\text{m}}$ is 3 - 4, if a Gaussian atomic velocity distribution is assumed. At IRc2, the calculated optical depth of the 63 μm O I line is somewhat larger, 4 - 5.5. These O I optical depths are in good agreement with those calculated from the peak antenna temperatures of the O I and C II lines throughout the range of temperatures derived above.

The intrinsic linewidth in the PDR is small, $\sim 4.5\ \text{km s}^{-1}$ (FWHM) near $\theta^1\text{C}$ and $\sim 3.6\ \text{km s}^{-1}$ at IRc2, after correction for the optical depth in the fine-structure lines. This value agrees well with that seen in carbon recombination lines in the same region ($4.4\ \text{km s}^{-1}$; Jaffe and Pankonin 1978). We see no evidence for a broad velocity component at $\theta^1\text{C}$, although as can be seen from Fig. 1, there is an additional velocity component near $3\ \text{km s}^{-1}$, at least in the 158 μm C II data. At IRc2, both the C II and O I lines are asymmetric, which indicates a contribution to the emission from material associated with the molecular ridge at a velocity near $10\ \text{km s}^{-1}$ in addition to that from photodissociated gas at $V_{\text{LSR}} \sim 8\ \text{km s}^{-1}$. An upper limit (1σ) to the antenna temperature (T_r^*) of a broad emission component ($\Delta v_{\text{FWHM}} = 25 - 40\ \text{km s}^{-1}$) is 6 K for O I. Any broad emission, presumably from shock-excited gas, could contain an integrated intensity equivalent to that in the narrow component (listed in Table 1), as suggested by the data of Crawford et al. (1986) and Werner et al. (1984). However, the measured line width (FWHM) remains unaffected by the broad component.

4.3. Comparison with PDR Models and Previous Measurements

The PDR model of Tielens and Hollenbach (1985a, 1985b) solves equations of chemical equilibrium and energy balance to calculate temperature and number density profiles through a photodissociation region illuminated by UV radiation. Their best-fit model for the $\theta^1\text{C}$ region has densities $n_{\text{H}} = 1 \times 10^5\ \text{cm}^{-3}$ and a peak temperature near 550 K. The parameters, however, are determined from integrated intensity measurements of O I and C II emission and assumed identical line widths of $4.5\ \text{km s}^{-1}$ (FWHM), which are smaller than the true (and different) values for O I and C II, as can be seen from Table 1 and Fig. 1. Thus the gas kinetic temperature of 265 K calculated by Tielens and Hollenbach (1985b) for the moderately optically thick O I line is too high.

There are several advantages to determining temperature and density from the peak emission of spectrally well-resolved lines rather than from the integrated intensity. There is no confusion from different velocity components, which can affect comparisons of integrated intensity. For example, Fig. 1 shows a $3\ \text{km s}^{-1}$ component prominently in the C II data, but only weakly (if at all) in the O I 63 μm spectrum. This feature contributes 10% to the total integrated intensity in the C II line but is clearly irrelevant to the determination of physical parameters of the main $10\ \text{km s}^{-1}$ component of the PDR. Inclusion of this component in an assumed $5\ \text{km s}^{-1}$ linewidth

leads to a brightness temperature $T_B \sim 165$ K for C II, as calculated by Stacey et al. (1993) rather than 138 K, as seen in Table 1. The difference is not very significant in this case, but other locations within the Orion complex show line profiles with large asymmetries and additional velocity components.

The effect of reference beam emission is less severe for peak temperature measurements than for integrated intensity if velocity differences exist between the desired and potentially contaminating emission. Even with no velocity gradient, the 12.5 chop throw for the C II observations limits the reduction of our peak C II T_r^* to less than 10%, calculated from the strip scan of Stacey et al. (1993). The good agreement between our measured integrated intensity and that shown in this strip scan (which is corrected for self-chopping) also suggests that there was little emission in our reference beams. No reduction of the peak O I T_r^* is likely from reference beam emission, as shown by the O I map of Werner et al. (1984). Thus our conclusions remain substantially unchanged.

Finally, a single linewidth does not need to be assumed for all spectral features if they are resolved, so that line broadening from optical depth effects does not distort estimates of brightness temperature. Rather, the line width can be used as supporting evidence for the derived optical depth, as discussed in section 4.2.

Stacey et al. (1993) constructed a model for the PDR near θ^1 C based on 63 μm O I and 158 μm C II integrated intensity measurements. This model is characterized by a kinetic temperature $T_{\text{kin}} \sim 300$ K, density $n_{\text{H}} \sim 4 \times 10^5 \text{ cm}^{-3}$, and column density $N_{\text{H}} \sim 1.5 \times 10^{22} \text{ cm}^{-2}$. Since the O I and C II integrated intensities of the present data agree well with those used by Stacey et al. (1993), it is to be expected that those derived parameters which are independent of line width are also very similar in the two models. However, the 300 K derived kinetic temperature of Stacey et al. (1993) is significantly higher than ours ($T_{\text{kin}} = 175 - 220$ K) because they assumed the linewidth of the 63 μm O I line to be 5 km s^{-1} , similar to that of the C II, while the true value is near 6.8 km s^{-1} because of optical depth broadening, as seen in the present data. Spectrally resolved observations of the 145 μm $^3P_0 - ^3P_1$ O I line should further constrain estimates of the temperature and density of the Orion PDR.

The peak optical depth of the 158 μm C II line of ~ 0.9 calculated by Stacey et al. (1993) is lower than that obtained from the present data because of the difference in model kinetic temperatures, while the 63 μm O I line has comparable model optical depths. From comparison of the integrated intensity of the F=1-0 hyperfine component of the 158 μm ^{13}C II fine-structure line with that of the ^{12}C II line, Stacey et al. (1991) obtained a relationship between the line-averaged ^{12}C II optical depth and the $^{12}\text{C}/^{13}\text{C}$ isotopic ratio R :

$$\frac{\tau}{1 - e^{-\tau}} = 1.45_{(-0.24)}^{(+0.34)} \cdot \frac{R}{43}$$

at θ^1 C. For their assumed isotopic ratio of 43, the corresponding peak optical depth is $1.2_{(-0.6)}^{(+0.7)}$, in agreement with the range of 1.0 - 1.3 derived in this paper.

We thank the staff of the Kuiper Airborne Observatory for their consistent support, especially during the stressful last month of KAO operations. This work is supported by NASA grant NAG 2-753.

Table 1. Observed O I and C II Line Parameters^a

Position	V_{LSR} (km s^{-1})	Linewidth (km s^{-1} , FWHM)	Peak T_r^* (K)	T_{B} (K)	Integrated Intensity ($\text{erg cm}^{-2} \text{s}^{-1} \text{sr}^{-1}$)	Continuum T_r^* (K)
63 μm O I line ^b						
$\theta_1\text{C}$	9.8(0.2)	6.8(0.4)	76.8(5.1)	165(6)	$5.42(0.15)\times 10^{-2}$	0.4(0.3)
IRc2	8.5(0.2)	5.8(0.4)	54.7(6.4)	139(8)	$3.15(0.14)\times 10^{-2}$	4.2(0.3)
158 μm C II line ^c						
$\theta_1\text{C}$	9.9(0.1)	5.4(0.3)	97.4(1.6)	138(2)	$4.32(0.03)\times 10^{-3}$	1.0(0.1)
IRc2	8.4(0.2)	4.2(0.3)	74.6(0.6)	114(1)	$3.00(0.02)\times 10^{-3}$	5.0(0.1)

^aNumbers in parentheses represent 1σ uncertainties.

^bnarrow component only

^cIntegrated intensity includes several velocity components.

REFERENCES

- Betz, A. L., & Boreiko, R. T. 1989, *ApJ*, 346, L101
- Betz, A. L., & Boreiko, R. T. 1993, in *ASP Conf. Ser. 41, Astronomical Infrared Spectroscopy*, ed. S. Kwok, (San Francisco:ASP), 349
- Boreiko, R. T., Betz, A. L., & Zmuidzinas, J. 1988, *ApJ*, 325, L47
- Crawford, M. K., Lugten, J. B., Fitelson, W., Genzel, R., & Melnick, G. 1986, *ApJ*, 303, L47
- Fischer, C. F., & Saha, H. P. 1983, *Phys.Rev.A*, 28, 3169
- Henningsen, J. O., & Petersen, J. C. 1978, *Infrared Phys.*, 18, 475
- Jaffe, D. T., & Pankonin, V. 1978, *ApJ*, 226, 869
- Kutner, M. L., & Ulich, B. L. 1981, *ApJ*, 250, 341
- Launay, J. M., & Roueff, E. 1977, *A&A*, 56, 289
- Linsky, J. L. 1973, *ApJS*, 25, 163
- Melnick, G., Gull, G. E., & Harwit, M. 1979, *ApJ*, 227, L29
- Stacey, G. J., Jaffe, D. T., Geis, N., Genzel, R., Harris, A. I., Poglitsch, A., Stutzki, J., & Townes, C. H. 1993, *ApJ*, 404, 219-231
- Stacey, G. J., Smyers, S. D., Kurtz, N. T., & Harwit, M. 1983, *ApJ*, 265, L7
- Stacey, G. J., Townes, C. H., Poglitsch, A., Madden, S. C., Jackson, J. M., Herrmann, F., Genzel, R., & Geis, N. 1991, *ApJ*, 382, L37
- Storey, J. W. V., Watson, D. M., & Townes, C. H. 1979, *ApJ*, 233, 109
- Tielens, A. G. G. M., & Hollenbach, D. 1985a, *ApJ*, 291, 722
- Tielens, A. G. G. M., & Hollenbach, D. 1985b, *ApJ*, 291, 747
- Werner, M. W., Gatley, I., Harper, D. A., Becklin, E. E., Loewenstein, R. F., Telesco, C. M., & Thronson, H. A. 1976, *ApJ*, 204, 420
- Werner, M. W., Crawford, M. K., Genzel, R., Hollenbach, D. J., Townes, C. H., & Watson, D. M. 1984, *ApJ*, 282, L81
- Zink, L. R., Evenson, K. M., Matsushima, F., Nelis, T., & Robinson, R. L. 1991, *ApJ*, 371, L85

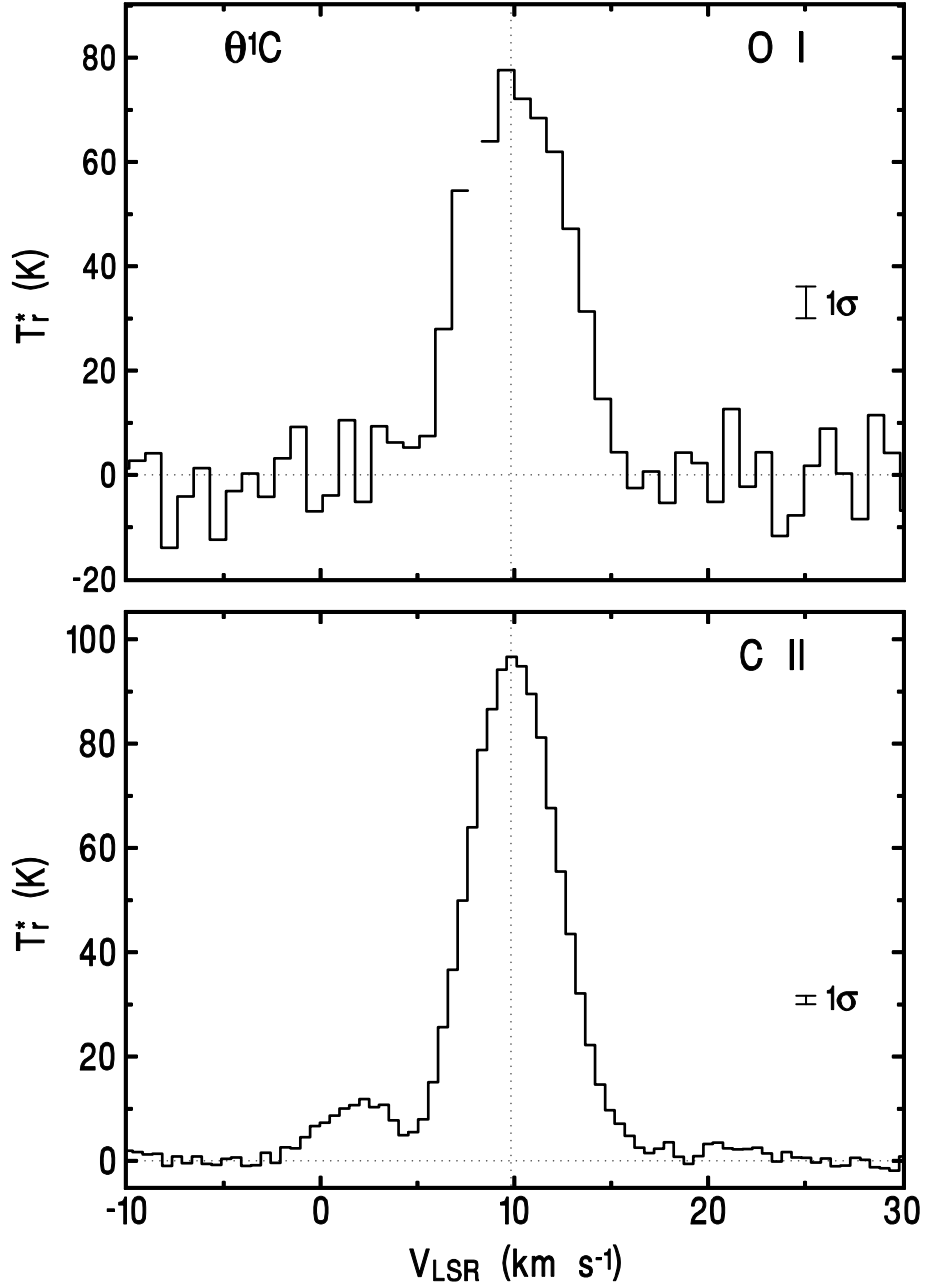


Fig. 1.— Observed spectra of the $63 \mu\text{m}$ O I and $158 \mu\text{m}$ C II fine-structure lines toward $\theta^1\text{C}$. Integration times are 72 minutes for O I and 12 minutes for C II. The continuum has been removed from both spectra. The light vertical line is at $V_{\text{LSR}} = 9.8 \text{ km s}^{-1}$. The gap in the O I spectrum near $V_{\text{LSR}} = 8 \text{ km s}^{-1}$ shows the region where telluric atomic oxygen absorption exceeds 50%.

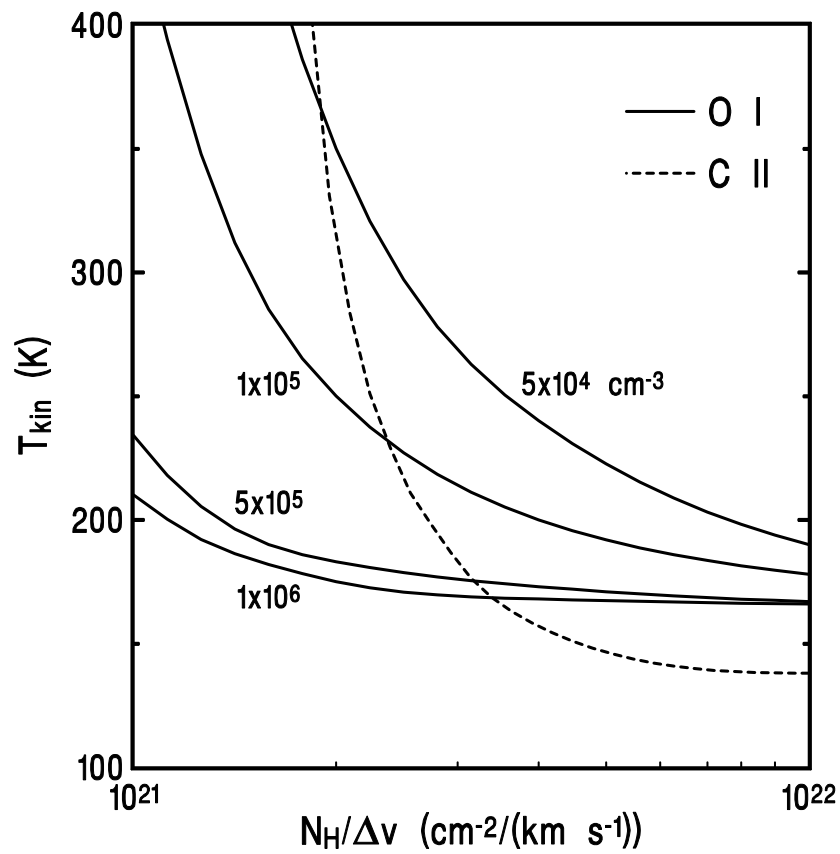


Fig. 2.— Combinations of gas kinetic temperature and hydrogen column density per unit velocity interval which produce the observed O I $63 \mu\text{m}$ (solid lines) and C II $158 \mu\text{m}$ (dashed line) peak antenna temperatures at $\theta^1\text{C}$. The O I curves are calculated for various gas densities. See text for details.